Interpreting the Time-Resolved Photoluminescence of Quasi-2D Perovskites

Milian Kaiser, Yang Li, Isabel Allegro, Bryce S. Richards, Ulrich Wilhelm Paetzold,* and Ian A. Howard*

Optical excitation of quasi-2D perovskites leads to excited-state populations of excitons, free charge carriers, or a mixture of both, depending on the type and amount of 2D spacer used. The fluence dependence of three quantities: 1) the time-resolved photoluminescence decay, 2) the photoluminescence quantum yield (PLQY) after pulsed excitation, and 3) the initial rate of photon emission, allow the mixture of excited states present to be determined. These can be described by a simple model considering noninteracting populations of excitons and charge carriers in separate subvolumes of the film. The model reproduces all unique features of the data, such as the anomalous peak of the PLQY at intermediate fluences, due to bimolecular free carrier emission gaining efficiency before exciton–exciton annihilation reduces the exciton emission efficiency. The excited state population varies from 100% excitons in films made from high concentrations of butylamine spacers to ≈7% excitons and 93% free carriers for low concentrations of 1-naphthylmethylamine spacers. The effective rates of free carrier recombination and exciton–exciton annihilation are high, often on the order of 1×10^{-9} cm^3 s^{-1}. The implications for the different excited-state populations and their dynamics in terms of device engineering are discussed.

1. Introduction

Quasi-2D perovskites use bulky organic cations, known as 2D-spacers, to create quantum wells (QWs) of varying thicknesses. A Ruddlesden–Popper quasi-2D perovskite has a general formula of $L_2(SMX_3)_{n-1}MX_4$, where M is a divalent metal cation, X is a halide, L is a large organic cation, and S can either be a small organic cation or a monovalent metal cation.[1–5] Finally, n represents the number of $[MX_6]^{4-}$ octahedral units across the QWs thickness. When $n = 1$ the material is truly 2D, whereas thicker quantum wells with $n > 1$ are referred to as

quasi-2D. For $n > 1$, usually, a distribution of QW thicknesses is present in the film. These multiple-quantum-well (MQW) structures are of interest for photovoltaic and light-emitting applications due to their stability, color purity, and high quantum efficiency.[3,5–15] For example, the external quantum efficiency (EQE) of perovskite light-emitting diodes (PeLEDs) based on MQW quasi-2D perovskites has reached 20%[15] utilizing iodide (800 nm emission) and over 15%[14] utilizing bromide (520 nm emission).

The photophysical properties of MQW structures are complex and important to understand in terms of engineering devices. The bandgaps of the QWs in an MQW film depend on their thickness, with smaller QWs having higher bandgaps and exciton binding energies due to their increased confinement.[16–20] The stronger coulombic effects between free charge carriers (FC, electrons and holes in continuum states) in thin (small-n) QWs will also increase the absorption coefficient of the FC absorption in these smaller QWs.[21] Therefore, for photoexcitation well above the bandgap, absorption from continuum states in smaller QWs should dominate. The excited states in these small QWs quickly transfer to the larger QWs in the system from which emission occurs.[7–9,22]

We will show herein that the emission from a quasi-2D perovskite film can be due to excitons, FC recombination, or indeed a mixture of both. We propose a simple model to account for this transition and the mixed nature of the excited-state population in quasi-2D perovskite films. Depending on the thicknesses of the local bandgap minima QWs to which the excited states are funneled, the excited-state population in these local minima QWs is either excitons or FCs. Whether the local minima are above or below a critical thickness (exciton binding energy) determines whether the excited states in that local minimum QW are dominantly FCs or excitons. If all local minima QWs are below this critical thickness, then the excitons dominate excited-state population in the film responsible for the emission. If all local minima QWs are above this critical thickness, then FCs account for the entire excited-state population of the film responsible for the emission. If the local minima lie on either side of this critical value, then a mixture of dominant exciton emission from some subset of QWs and dominant FC emission from another subset of QWs is observed. A schematic representation of these proposed photophysical mechanisms is presented in **Figure 1** and Figure S1 (Supporting Information),

M. Kaiser, Y. Li, B. S. Richards, U. W. Paetzold, I. A. Howard
Institute of Microstructure Technology
Karlsruhe Institute of Technology
Hermann-von-Helmholtz-Platz 1, 76344 Eggenstein-Leopoldshafen, Germany
E-mail: ulrich.paetzold@kit.edu; ian.howard@kit.edu
Y. Li, I. Allegro, B. S. Richards, U. W. Paetzold, I. A. Howard
Light Technology Institute
Karlsruhe Institute of Technology
Engesserstrasse 13, 76131 Karlsruhe, Germany

The ORCID identification number(s) for the author(s) of this article can be found under https://doi.org/10.1002/admi.202101326.
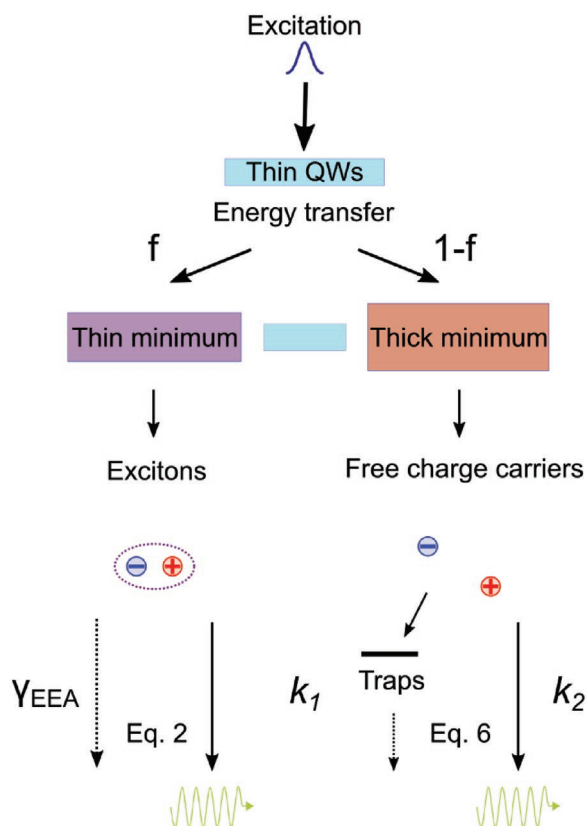
Figure 1. Schematic representation of how the excited states in a quasi-2D perovskite film responsible for emission can either be excitons, free charge carriers, or a combination of both. Here, f is the fraction of excitonic PL.

and this simple model considering two pools with independent rate equations will prove sufficient to self-consistently describe all experimental data we collect on the varying 2D spacers and their concentrations with reasonable accuracy.

Our analysis is based on the fluence dependence of three observables after pulsed excitation: namely, the photoluminescence (PL) decay kinetics, the rate of emission at time zero (PL$_0$), and the efficiency of the PL (PLQY). The paper is structured as follows. Section 2 introduces how the fluence-dependence of the three observables (PL kinetics, PL$_0$, and the PLQY) differs for systems in which excitons or FCs are exclusively responsible for the PL with rate equation simulations. Section 3 examines experimental data for perovskites based on *n*-butylamine (BA) and 1-naphthylmethylamine (NMA) spacers with the most distinct differences and show that these closely mimic the behavior for pure excitonic emission and pure free charge carrier emission presented in Section 2 (the quasi-2D films are prepared from a precursor solution, as described below, and of the form CsPbBr$_3$(NMA or BABr)$_x$ where x is varied from 0.4 to 1.0). Section 4 presents how the time-resolved photoluminescence (TRPL) changes when the amount of BA-spacer is reduced, demonstrating that FC recombination begins to play a measurable role alongside the excitonic emission. In Section 5, we show that when the concentration of NMA in the films is increased the PL$_0$ becomes increasingly less than quadratic. Nonetheless, the excited-state dynamics remain

dominated by FC emission, a large component of exciton emission cannot be invoked to explain the reduction in the slope of PL$_0$ with increasing NMA concentration. Instead, we suggest that in this case exciton–exciton annihilation (EEA) during the funneling processes must reduce the "initial" excited-state density in the bandgap-minima quantum wells. Finally, we comment on the limitations of this analysis and future challenges to overcome in the understanding of TRPL transients from quasi-2D perovskites, and also on the impact of this understanding concerning device engineering.

2. Simulation: Excitonic versus Free Charge Carrier PL

Here we theoretically introduce the simple model for light emission in quasi-2D perovskites that we will use to interpret the experimental data in the following sections. The model will consider two independent populations of excitons and charge carriers supported in separate regions of the film due to the inhomogeneity of the local minimum QW bandgaps. As an aside to the interested reader, the alternative model that considers coupling between the exciton and charge carrier populations in local minimum QWs of a more homogeneous QW depth fails to explain the observed data. For one, the observed dominance of excitonic emission at long times (and therefore low excited-state densities) is inconsistent with this alternative model as it would predict the excited-state density become dominated by FCs as the excited-state density is lowered and therefore a shift in the spectrum takes place. This is not observed. Therefore, although we do not propose that the simplistic two-pool model captures all photophysical processes rigorously, we do suggest that it is the simplest model to reproduce the salient features of the dataset accurately and as such has utility in beginning the interpretation of PL dynamics in quasi-2D perovskites.

As introduced above, excited states are most likely to be formed in the thinner QWs, due to the coulombic enhancement of the continuum absorption in these wells with higher exciton binding energies.[21] As shown in Figure 1, we propose that these excited states (likely primarily excitons) then funnel quickly into larger quantum wells that represent local bandgap minima and are widely enough separated by higher bandgap material that the transport between the local-minima QWs is poor. If a local minimum QW is thinner than a critical value (which also could depend on the nature of the 2D ligand), then the excitons are stable in this bandgap minimum. If, on the other hand, a bandgap-minimum QW is thicker than this critical value, the exciton can separate into FCs, and the excited-state dynamics in these QWs will be dominated by FC recombination.

In the case of excitonic recombination, the exciton density can be described as

$$\frac{dn_x}{dt} = -k_x n_x - \gamma_{EEA}(t) n_x^2 \tag{1}$$

where k_x is the total monomolecular rate constant including radiative and nonradiative contributions, $k_x = k_{x,\,rad} + k_{x,nrad}$ and
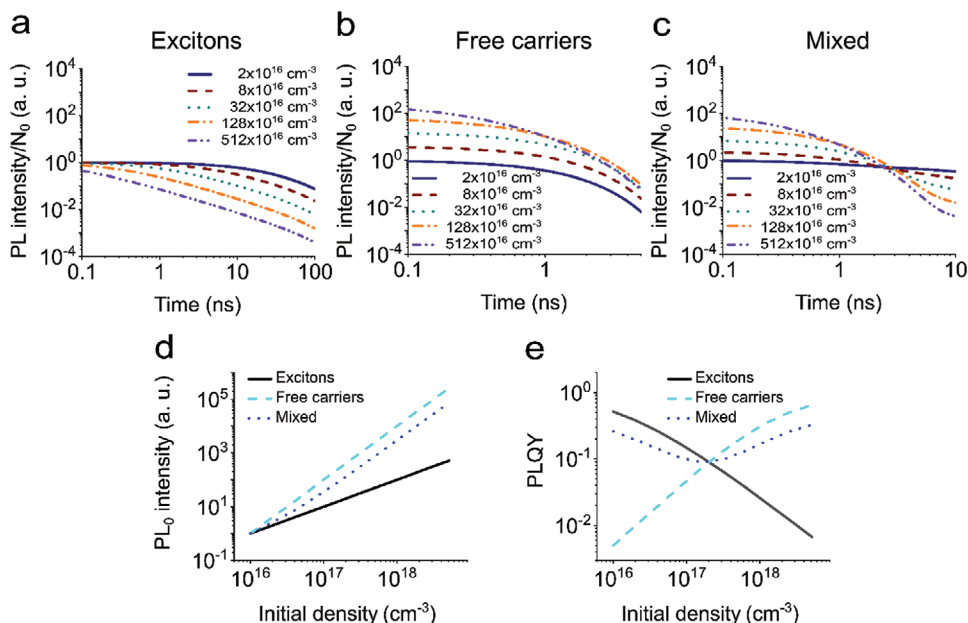
Figure 2. Simulations to illustrate the PL kinetics divided by the initial excited-state density N_0 of a) excitons b) free carriers (FCs) and c) a 50/50 mixture ($f = 0.5$) of exciton and FC PL. Simulations of d) the PL_0 and e) PL efficiency of excitons, FCs, and a 50/50 PL mixture dependent on excitation fluence.

γ_{EEA} is the rate constant for bimolecular EEA. When excitons can diffuse without constraint in two or three dimensions, then $\gamma_{EEA}(t)$ can be considered as a constant, $\gamma_{EEA} = 8\pi D R_{crit}$, related to the exciton's diffusion coefficient, D, and the radius at which two excitons interact, R_{crit}. For the illustration in **Figure 2**, we select $\gamma_{EEA} = 2.5 \times 10^{-9}$ cm^3 s^{-1}, a value following recent literature.[23] For k_x, we take 1.25×10^7 s^{-1}, a monomolecular lifetime similar to those typically measured in quasi-2D perovskites based on phenethylamine or BA ligands with high 2D spacer content.[23]

In a TRPL measurement, such as time-correlated single-photon counting or streak camera measurements, the numbers of photons arriving in given time windows after excitation are collected. The number of photons counted in each time window after excitation gives the rate of photon emission at that time (i.e., the number of photons emitted divided by the length of the time window is the rate of photon emission at a given time delay). In the case of exciton emission, the rate of PL emission as a function of time can be expressed as

$$PL_x(t) \propto k_{x,rad} n_x(t) = k_x \left(\frac{k_{x,rad}}{k_{x,rad} + k_{x,nrad}} \right) n_x(t)$$

$$= k_x \, \phi \, \frac{k_x}{\gamma_{EEA}(\exp(k_x t) - 1) + \frac{k_x}{N_0} \exp(k_x t)} \quad (2)$$

where φ is the radiative fraction of the total decay. In this excitonic case, the measured PL dynamic is directly proportional to the excited-state population density at a given time. As shown, the integral form of Equation (1) gives an explicit expression for $n_x(t)$, where N_0 is the initial exciton density. Unfortunately, the initial exciton density inside energy minima QWs is not easily accessible, as the volume fraction of the film occupied by these energy minima QWs is not easy to assess. Therefore, herein we

will underestimate N_0 as the average density of excited states created inside the film as calculated from the excitation fluence, sample absorbance, and film thickness. This will mean that the extracted values for γ_{EEA} are effective values based on the underestimated N_0. If the real, higher density in the energy minima QWs were known, then the actual rate constants in the individual QWs could be calculated, and these would be lower than the effective γ_{EEA} values quoted here. We note that this is a general challenge to the interpretation of TRPL transients in these quasi-2D systems, and will be discussed further later. Finally, we point out that Equation (2) considers that exciton transport between energy-minima QWs is possible whereas in our physical model this should not be the case. As long as the number of excitons per energy minima QW is initially high, as must be the case for the EEA rates observed at the higher fluences herein, this is not an issue. A more nuanced model considering the role of finite domain sizes would be possible to develop but would introduce parameters (such as domain size) that would be impossible to constrain from the current data. In this first analysis, we, therefore, note the small inaccuracy introduced by the equation allowing transport between all QWs supporting excitons but demonstrate that the equations as presented are a reasonable enough approximation to be a useful first step.

Immediately after impulsive excitation, assuming that there has not been enough time for EEA to occur, then

$$PL_x(0) = k_x \, \phi \, N_0 \quad (3)$$

From Equation (3), it can be seen that the excitonic PL at zero-time, $PL_x(0)$, will scale linearly with the initial excitation density (i.e., also linearly with the excitation fluence) as long as EEA during the instrument response time can be neglected. EEA during the instrument response time leads to the convolution of the instrument response function and the PL dynamics,

**ADVANCED
SCIENCE NEWS**

www.advancedsciencenews.com

**ADVANCED
MATERIALS
INTERFACES**

www.advmatinterfaces.de

effectively decreasing the measured maximum PL intensity at zero time. The measured PL maximum can be approximated as $PL_{I.R.} = PL(t_D)$, the PL after a small time delay (t_D), which is roughly half the instrument response time.

Finally, the quantum yield in the excitonic case can be found as the number of emitted photons divided by the number of initial excitations. The number of emitted photons is the integral of Equation (2)

$$PLQY_x = \frac{\int_0^\infty k_{x,\text{rad}} n(t)\, dt}{N_0} = \phi \frac{-k_x}{\gamma N_0} \ln\left(\frac{k_x}{k_x + \gamma N_0}\right) \quad (4)$$

Looking at the limits of Equation (4), when $N_0 \to 0$, then $PLQY_x \to \varphi$. That is, at small initial excitation densities, linear processes dominate, and the quantum efficiency is simply given by the competition between monomolecular radiative and nonradiative channels. On the other hand, when $N_0 \to \infty$, then $PLQY_x \to 0$. When excitation density increases, the PLQY of the exciton emission is decreased due to increased nonradiative loss caused by EEA. We note that this agrees with the simplified estimation for the PLQY using the estimation that the rate of annihilation stays at its maximum rate throughout the decay. This leads to an approximation for the PLQY as $\phi \frac{k_x}{k_x + \gamma N_0}$, which is a slight underestimate due to exaggeration of the bimolecular recombination fraction. A comparison of the PLQY as a function of N_0 for the simple approximation and Equation (4) is shown in Figure S2 of the Supporting Information.

If excitation leads to FCs, the PL dynamics, PL_0, and PLQY all scale differently with fluence. In this case, and assuming an intrinsic semiconductor where the number of electrons in the conduction band is equal to the number of holes in the valence band after photoexcitation, the number of electrons in the conduction band density evolves with time as

$$\frac{dn_c}{dt} = -k_{1,c} n_c - k_{2,c} n_c^2 \quad (5)$$

where n_c is the electron density, $k_{1,c}$ is the rate of monomolecular nonradiative loss (i.e., due to charge-trapping), and $k_{2,c}$ is the bimolecular rate of electron–hole encounter leading to radiative decay. In this case, we ignore third-order Auger recombination, as we are interested in understanding the PL dynamics in a fluence range before this third-order effect sets in.

The photon emission rate as a function of time for FC-based emission is then given by

$$PL_c(t) = k_{2,c} n_c(t)^2 = k_{2,c} \left(\frac{k_{1,c}}{k_{2,c}\left(\exp(k_{1,c}t) - 1\right) + \frac{k_{1,c}}{N_0}\exp(k_{1,c}t)}\right)^2 \quad (6)$$

where N_0 represents the initial density of electrons within the bandgap minima QWs supporting FCs. As noted above, the actual local density inside the energy minima QWs is currently impossible to estimate, as the volume fraction of the total film

of the energy minima QWs is unknown. This leads to an effective rate for $k_{2,c}$ as well, which will be higher than the real rate.

The rate of emission at zero-time for FC-based emission can be simply found from Equation (6) as

$$PL_c(0) = k_{2,c} N_0^2 \quad (7)$$

This means for the case of FC emission, the rate of PL emission at zero-time will scale with the square of the initially created carrier density (or equivalently the excitation fluence).

Finally, the PLQY from FC emission is

$$PLQY_c = \frac{\int_0^\infty k_{2,c}\left(n_c(t)\right)^2 dt}{N_0} = \frac{\left(k_{2,c} N_0 + k_{1,c}\ln\left(\frac{k_{1,c}}{k_{1,c} + k_{2,c}N_0}\right)\right)}{k_{2,c}N_0} \quad (8)$$

For FC emission, looking at the limits of Equation (8), when $N_0 \to 0$, then $PLQY_c \to 0$. That is, at small initial excitation densities, the linear trapping processes dominate and the quantum efficiency is negligible. On the other hand, when $N_0 \to \infty$, then $PLQY_c \to 1$. When excitation density increases, the PLQY of the emission increases, and in this case (where higher-order Auger loss is neglected) goes to unity. Similarly to the above case for excitons, an approximation for the PLQY of FC emission can be made assuming that the bimolecular recombination maintains its initial rate throughout the whole decay. In this case, the PLQY would be $\frac{k_{2,c}N_0}{k_{2,c}N_0 + k_{1,c}}$, and it would be slightly overestimated due to the exaggeration of the role of bimolecular decay. Again, a comparison of the PLQY as a function of fluence for Equation (8) and the simplification is presented in Figure S3 of the Supporting Information.

Finally, a mixture of excitonic PL and PL based on FC recombination coming from independent population pools can be expressed by combining the already established equations. From Equations (2) and (6) using f as the fraction of the bandgap-minima QWs that support excitons

$$PL = f PL_x + (1 - f) PL_c \quad (9)$$

Consequently, it follows from Equations (3) and (7)

$$PL(0) = f PL_x(0) + (1 - f) PL_c(0) \quad (10)$$

And from Equations (4) and (8)

$$PLQY = f PLQY_x + (1 - f) PLQY_c \quad (11)$$

We note that that the initial excited-state density, N_0, will be the same for PL_x and PL_c irrespective of f. The density of states inside subfractions of the total volume is the same, but the comments above about the underestimation of N_0 based on the total film volume still apply.

Having now established how the PL dynamics, zero-time PL, and PLQY scale with the initial excited-state density for exciton

**ADVANCED
SCIENCE NEWS**

www.advancedsciencenews.com

**ADVANCED
MATERIALS
INTERFACES**

www.advmatinterfaces.de

and FC populations, we present a comparison of these characteristics in Figure 2 for exemplary parameters. As previously stated, for the exciton emission the total monomolecular exciton decay rate used is 1.25×10^7 s^{-1}, consistent with Delport et al.[23] The EEA rate used is 2.5×10^{-9} cm^3 s^{-1}, this is consistent with the value of 2.5×10^{-4} cm^2 s^{-1} obtained by Delport et al.[23] for a 100 nm film thickness. The parameters used for the illustration of the charge carrier recombination are roughly based on the results for NMA$_{0.4}$ below and are $k_{1,c} = 5 \times 10^8$ s^{-1} and $k_{2,c} = 5 \times 10^{-10}$ cm^3 s^{-1}.

We simulate the initial excited-state densities from 1×10^{16} to 5×10^{18} cm^{-3}, which corresponds to excitation fluences of 0.2 to 95 µJ cm^{-2} for a 100 nm thick film absorbing 30% of the incident photons with a wavelength of 350 nm.

In Figure 2a–c we plot the TRPL intensity divided by the initial excited-state density for excitons, free charge carriers, and a mixture of the two, respectively. That is Equations (2), (6), and (9) all divided by N_0. The division by N_0 is better than simply plotting the PL intensity for distinguishing excitonic and FC-based emission. Looking at the PL intensity alone, or normalized to its maximum value, the shortening of the lifetime with increased fluence looks similar for both free charge carrier and excitonic emission (see Figure S4, Supporting Information). However, the two cases look quite different when the PL dynamics are normalized to the initial excited-state density. For excitonic emission, the PL decays divided by the initial excited-state density always start at the same point (given no EEA occurs within the instrument response of the system). For low fluences, the excitonic decays continue to lie directly on top of one another. The efficiency of the emission in these cases is the same (Figure 2e). For FC emission, the PL decays normalized to the lowest N_0 do not start at the same point. As the fluence is increased, the FC emission curves start at higher values (due to the quadratic scaling of PL$_0$). This leads the curves to be offset from one another. Figure 2d,e presents the initial rate of emission alongside the PLQY for the two cases. The slope of PL$_0$ on a log–log scale is one versus two for excitonic versus FC emission. The PLQY of the FC emission monotonically increases with fluence, whereas that of the excitons monotonically decreases.

Having established that FC and excitonic emission are easily distinguishable from the examination of these three metrics, we now turn to consider how the data may look when both exciton and FCs would exist in separate volumes of the film. In Figure 2c we show the PL intensity divided by N_0 for dynamics for $f = 0.5$. For increasing excitation fluence the early emission monotonically increases like the FC case, however, the magnitude of the spread of the initial point from low to high fluence is less than in the pure FC case. Interestingly, at some time after the excitation, the curves cross, with higher fluence curves moving from lying above to lying below a lower fluence curve. Such crossing behavior is not observed for pure exciton dynamics. In pure FC dynamics weak crossing is observed at high excitation fluences, but will be seen much more dominantly in some of the experimental data below. In Figure 2d we see that the slope of PL$_0$ starts below two but reaches two at higher fluences. The low-fluence PL is dominated by exciton recombination due to the linear dependency of PL on the exciton density. The PL at higher fluences

however is dominated by FC recombination. This change in which species is dominating the PL dynamics is even more pronounced in the PLQY shown in Figure 2e which uniquely does not exhibit a monotonic trend with fluences. In this case, the PLQY decreases with increasing fluences while exciton PL is dominating and EEA reduces its efficiency. As the excitation fluence becomes higher the increased bimolecular recombination from the FC population causes the quantum yield to rise again. Equally possible (with other rate constants) would be an increase in PLQY at first, due to FC emission becoming more efficient, then a subsequent drop due to EEA reducing the efficiency of the excitonic emission.

3. Experimental Observations of Exciton- and FC-Dominated PL

In previous work, we examined the amplified spontaneous emission (ASE) thresholds of quasi-2D perovskites as a function of 2D spacer and content.[24] We found that ASE thresholds for materials whose emission mechanism appeared more excitonic (based on analysis of PL$_0$) were worse than those whose emission mechanism appeared more based on FC recombination. In this work, we revisit the same series of quasi-2D materials made from varying fractions of BA or NMA 2D-spacers to analyze the differing photophysics in these series more closely and to more fully understand what excited-state species are present and responsible for the highly varying TRPL observations.

In **Figure 3** we consider the TRPL of the two samples most analogous to pure excitonic emission and pure FC-recombination based emission, namely, the perovskite with $\gamma = 0.4$ NMA spacer (NMA$_{0.4}$) and the perovskite with $\gamma = 1.0$ BA spacer (BA$_{1.0}$). For BA$_{1.0}$, the PL dynamics divided by the initial
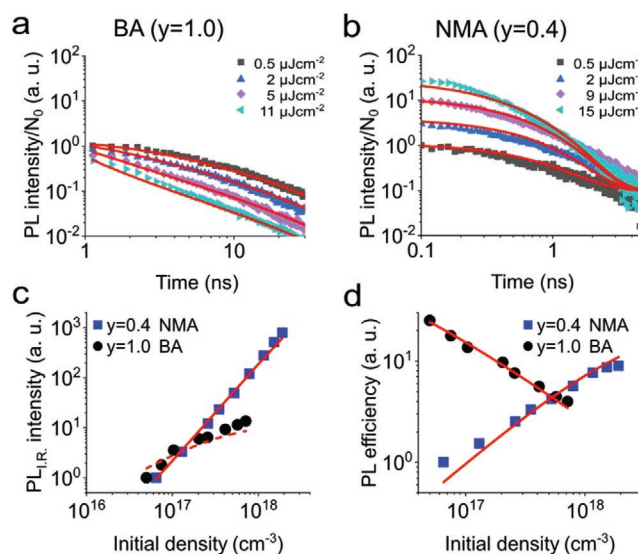
Figure 3. Time-resolved PL dynamics divided by the initial excited-state density for the a) BA$_{1.0}$ perovskite and b) NMA$_{0.4}$ perovskite at different fluences and fitted with Equations (2) and (9) divided by N_0, respectively. c) PL$_{I.R.}$ fitted with Equations (2) and (9) and d) PL efficiency of the NMA$_{0.4}$ and the BA$_{1.0}$ perovskites fitted with Equations (4) and (11), respectively, utilizing the same parameters as in (a) and (b).

excited-state density (which is assumed to be linearly proportional to the excitation fluence) are presented in Figure 3a. These data are also all divided by a common factor so that the initial point of the lowest fluence curve becomes one, for clarity of presentation. This will also be done for all further datasets to aid comparison. Also, to show the complete PL dynamics data on a log-log graph the maximum signal height of the measured TRPL is assigned a time value of 1.1 ns, this will be done for all BA samples. For fluences from 0.5 to 11 μJ cm^{-2} the PL decays become faster with increasing fluence. At fluences above 5 μJ cm^{-2} not only does the initial decay become increasingly fast, but also the initial points in Figure 3a start dropping below those of lower fluences. This is also seen in Figure 3c where PL_0 starts to scale sublinearly with fluence. These deviations from the ideal data shown in Figure 2 are simply a consequence of the finite instrument response of the Streak system (≈1 ns on the time range used for these measurements), and some EEA occurring within the instrument response of the system. This annihilation within the instrument response at the higher fluences explains why the initial points can no longer scale linearly with fluence and drop below those of lower fluences. We note this is the exact opposite to the behavior expected for FC recombination, wherein the initial points at higher fluences will be above the initial points at lower fluences. As introduced above we interpret these PL values as the PL shortly after zero-time. We, therefore, take the zero time for our model to be roughly half the instrument response time (0.68 ns) earlier than the maximum PL signal (1.1 ns). Instead of using Equation (3) to model PL_0, which would be correct with an infinitely short instrument response, we take the modeled emission rate at the delay time corresponding to the maximum of the observed data. This "effective" PL_0 taking into account the finite instrument response is labeled as $PL_{I.R.}$ rather than PL_0 for the sake of clarity. As shown in Figure 1a,c, this procedure to account for the instrument response allows for an excellent estimation of the dynamics and slope of $PL_{I.R.}$.

Finally, considering Figure 3d, we see that the PLQY monotonically decreases with increasing fluence for BA$_{1.0}$. All these observations are in complete accordance with the qualitative expectations for excitonic decay. Finally, we fit the data with Equation (2) (normalized by N_0). The model for pure exciton recombination fits the data extremely well over a variety of fluences as demonstrated in Figure 3a. The extracted parameters are $k_x = 2.7 \times 10^7$ s^{-1} and $\gamma_{EEA} = 6 \times 10^{-9}$ cm^{-3} s^{-1}. We note as discussed above, that γ_{EEA} is an effective rate. The actual rate of γ_{EEA} will be somewhat lower given the actual density will be higher. Nonetheless, encounter and annihilation rates will remain the same, i.e., the product of the effective rate coefficient and the uniformly distributed density will be the same as the product of the real rate coefficient and real density. The PL_0 and PL efficiency as a function of fluence is also well reproduced using these parameters as shown in Figure 3d.

Turning to the NMA$_{0.4}$ data displayed in Figure 3b we see a clear increase in the early PL divided by the initial excited-state density with excitation fluence. Due to the faster decay of the PL, we choose to locate the maximum at 0.1 ns from the NMA data to optimize visualization on a log–log scale, this is purely a cosmetic consideration. The slope of PL_0 shown in Figure 3c is almost exactly two which shows that the early

PL is dominated by FC recombination. The monotonically increasing efficiency shown in Figure 3d confirms that FCs are the main contributor to the PL. These features are in stark contrast to those observed in the BA sample and are direct evidence that the excited-state populations are drastically different in these materials.

The long tail of the TRPL dynamics for NMA$_{0.4}$ shown in Figure 3b cannot be fitted without some small contributions from exciton dynamics. We note that the time axes of Figure 3a,b are different, with the FC-dominated decay shown in Figure 3b being much shorter-lived. The TRPL dynamics of NMA$_{0.4}$ suggest that there is a small fraction of PL from excitonic recombination that makes up the longer-lived emission after the FC emission decays. We, therefore model these dynamics with Equation (9). The fractions of the PL are estimated to be 93% FC and 7% excitonic (we note to make this rough estimation we assume that the exciton emission efficiency is 100%, see note in the Supporting Information on how these estimates are affected by the excitons emission efficiency). For the FC emission, we extract $k_1 = 7.4 \times 10^8$ s^{-1} and $k_2 = 4.7 \times 10^{-10}$ cm^3 s^{-1}. As noted before k_2 is an effective rate constant, as the true microscopic N_0 is not accessible, but the product of this effective k_2 and the underestimated N_0 does lead to the correct recombination rate. The rate of FC loss due to trapping is fast with a lifetime of 1.35 ns, explaining the fast PL decay even at low fluences. For FC emission to be efficient $N_0 > \frac{k_1}{k_2} = 1.6 \times 10^{18}$ cm^{-3}. This explains why the efficiency of the PL carries on increasing up to these very high initial densities in this case, as shown in Figure 3d (wherein again the PLQY as a function of fluence for the extracted parameters matches the experimental data well). Finally, a monomolecular exciton rate, $k_x = 6 \times 10^7$ s^{-1} is extracted, which is twice the rate extracted for the BA film but still in reasonable agreement. With the minor contribution of exciton emission, fitting γ_{EEA} in this case, was not sensible, it has a too minor effect on the dynamics to be well constrained and we fixed the EEA rate coefficient to zero for this extreme case. All extracted parameters are summarized in **Table 1**.

To summarize we show that the BA$_{1.0}$ and NMA$_{0.4}$ have significantly different responses to excitation with quantitative differences indicating that the PL in the former is dominated by exciton recombination, whereas that in the latter is dominated by FC recombination. These differences in the PL have a large impact on device understanding and engineering. Although both are quasi-2D perovskites, these materials must be considered completely different in terms of excited-state dynamics and therefore in terms of device engineering.

4. Alteration of the Excited-State Population with BA Concentration

Having established in the previous section how the excited-state population and dynamics can completely change in quasi-2D perovskites based on the nature of the 2D spacer, we now turn to examine whether and how the excited-state populations and dynamics can be changed by the amount of a given 2D spacer in quasi-2D perovskites.

Table 1. Extracted parameters of the fits demonstrated in Figures 3–5.

Quasi 2D-perovskite	f [%]	$k_x \times 10^7$ [s^{-1}]	$\gamma_{EEA} \times 10^{-10}$ [cm^3 s^{-1}]	$k_{1,c} \times 10^7$ [s^{-1}]	$k_{2,c} \times 10^{-10}$ [cm^3 s^{-1}]
NMA$_{0.4}$	7 ± 3	6 ± 3	$0^{a)}$	74 ± 2	4.7 ± 0.2
NMA$_{0.6}$	22 ± 1	27 ± 2	2.4 ± 0.3	36 ± 2	13.0 ± 0.4
NMA$_{0.8}$	$0^{a)}$	–	–	141 ± 4	31 ± 2
NMA$_{1.0}$	$0^{a)}$	–	–	86 ± 2	50 ± 1
BA$_{0.4}$	42 ± 1	2.6 ± 0.2	0.75 ± 0.05	4.9 ± 0.7	3.7 ± 0.2
BA$_{0.6}$	52 ± 2	3.9 ± 0.2	1.7 ± 0.1	7 ± 1	8.4 ± 0.5
BA$_{0.8}$	77 ± 2	4.7 ± 0.2	4.8 ± 0.2	6 ± 4	19 ± 2
BA$_{1.0}$	$100^{a)}$	2.7 ± 0.1	60 ± 1	–	–

a)Constraint to allow for sensible fits.

In **Figure 4**a we show the PL dynamics with decreasing concentration of the BA spacer in the perovskite films. For the high contents of BA, BA$_{1.0}$, and BA$_{0.8}$, the initial point of the TRPL curves normalized by initial density stays the same or decreases at higher fluences due to EEA within the instrument response. This is a clear indication that the excited-state population is dominated by excitons. However, as the BA contents decrease to BA$_{0.6}$ and BA$_{0.4}$, the initial point on the TRPL curves normalized to the initial density becomes higher at the higher fluences, a direct indication that FC emission must now also play a significant role in these materials. Also, for BA$_{0.6}$ and BA$_{0.4}$, the curves with different excitation fluences shown in Figure 4a begin to cross, with higher fluence curves starting higher and ending lower than lower fluence curves. For pure excitonic emission (or pure FC emission for that matter) the curves do not cross. Thus, the qualitative observation of the crossing curves is direct evidence that as the BA content is decreased (causing QWs to become larger on average) the excited-state population responsible for emission moves from only excitons to a mixture of excitons and FCs. This is direct evidence that the nature and dynamics of the excited-state population depend not only on the nature of

the 2D spacer but also on the amount of a given 2D spacer in the material.

The dynamics of BA$_{1.0}$ were already modeled, but now we fit the dynamics of all other BA concentrations to the general mix of exciton and FC emission presented in Equation (9). The summary of extracted parameters is again presented in Table 1. First, the fraction of excitonic PL gradually decreases from 77% to 52%, then 42% for BA$_{0.8}$, BA$_{0.6}$, and BA$_{0.4}$, respectively. Another notable trend is observed along with the series. The effective rate coefficients corresponding to bimolecular interactions, γ_{EEA} and k_2, both decrease with decreasing BA concentration. We suggest the following explanation for this observation. At high BA concentration, there is a large volume fraction of small QWs. Thus, at the high BA concentrations, the initial excited states are funneled into a rather small volume fraction of larger QWs from which the emission happens. This means that a significant underestimation is caused by taking the excited-state density within the energy minima quantum wells to be the average density across the whole film, and consequently, the effective bimolecular rates are significantly higher than the real microscopic ones to compensate for this. However, when a lower fraction of BA spacer is used, fewer small QWs are
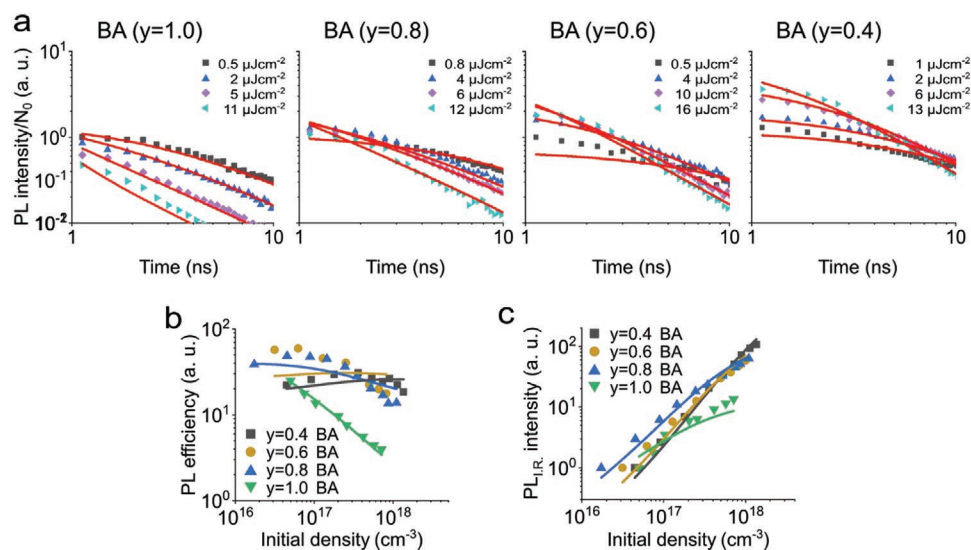
Figure 4. a) PL divided by the initial excited-state density of samples with different BA-spacer concentrations fitted with Equation (9) and below b) PL efficiencies and c) PL$_{I.R.}$ shortly after PL$_0$ of the same samples using Equations (9) and (11) with the same parameters as in (a).

formed and the emission can come from a greater volume fraction of the film. Therefore, the estimation of the initial N_0 may not be so far off, and the effective bimolecular rates observed may be closer to the real ones. The small emitting QWs at high BA concentrations additionally lead to stronger confinement, which causes a slight blue-shift in the emission (see Figure S6, Supporting Information). While this contributes to the higher bimolecular rates we assume the increase in N_0 to be the more dominant process. We note that further work must be done to check this hypothesis.

5. Effect of NMA Concentration on Photophysics

In **Figure 5**a we show how the TRPL dynamics for the NMA perovskites change as the NMA concentration increases. At first glance, there may be a direct analogy to the BA series shown in Figure 4. As the amount of NMA increases, the initial points of the TRPL emission normalized by excited-state density become less spread out. The initial points at high fluence are no longer so much higher than the initial points at the lower intensity. This could suggest an increasing contribution of excitons to the excited-state population. However, that would also necessitate an increasing contribution of the longer-lived exciton emission. Comparing the long-lived emission between NMA$_{0.4}$ and NMA$_{1.0}$, it is immediately apparent that there is not an increased contribution of a longer-lived signal for the NMA$_{1.0}$ data, interestingly the long-lived signal decays faster despite the initial points increasing significantly less than from NMA$_{0.4}$. The outcome of this is that this whole NMA series cannot be simply fit with Equation (9). Only the first two samples in the series, NMA$_{0.4}$ and NMA$_{0.6}$ can be adequately fit by Equation (9), with the fraction of excitonic PL increasing from 7% to 22%. Attempting a further increase in the exciton population to model the data for NMA$_{0.8}$, and NMA$_{1.0}$ (to account for the decrease in the slope of PL$_0$) leads

to inadequate fits for the dynamics (significantly overestimating the long-time PL).

The question then arises, how could the initial rate of emission not depend on the square of the excitation fluence (as necessary for FC emission), but despite this exciton emission not play a significant role in the dynamics? The answer that we propose relates to our observations of the increasing effective rate coefficients for bimolecular processes with increasing BA content. There, we suggested that the larger volume fraction of smaller QWs created with higher spacer concentrations led to a larger funneling effect and higher concentration of excited states in the sparser energy-minima QWs. A corollary of this is that it will take longer for the initial excitons to funnel into these sparser energy-minima QWs, and there could be more EEA during this energy transfer process. Thus, the initial density of excited states in the bandgap minima QWs might not scale linearly with pump fluence if EEA took place during the funneling process. This could contribute to the explanation of why the measured PL$_0$ slope for BA$_{1.0}$ is less than 1.0, and those for NMA$_{0.8}$ and NMA$_{1.0}$ are much less than 2.0.

To demonstrate the feasibility of such an explanation, we look at the excited-state population derived from the maximum PL of the NMA$_{0.8}$ and NMA$_{1.0}$ perovskites over the expected initial excited-state density. The loss in the excited-state population relative to the expected linear correlation is shown and discussed in Figure S5 of the Supporting Information. ASE in some of these materials can be observed at considerably higher excitation fluences than the ones used in this work. There are no ASE features, i.e., spectral narrowing observable in any of the spectra at the highest excitation fluences used in this work (see Figure S6, Supporting Information). Transparency cannot explain our observation, therefore, we are confident that the FC PL is always dominant for NMA-based quasi-2D perovskites, and we attribute the decrease of the slope of PL$_0$ with increasing NMA content to EEA
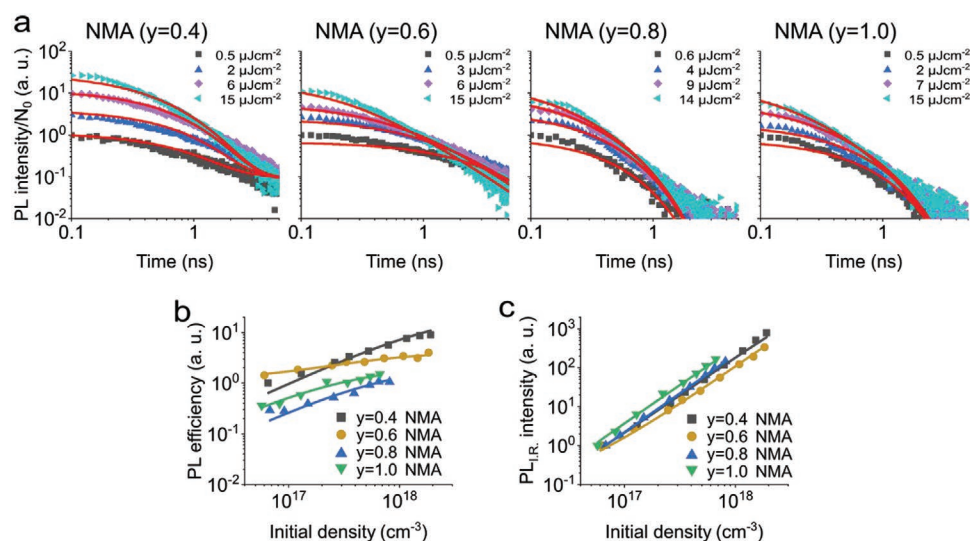
Figure 5. a) PL divided by the initial excited-state density of samples with different NMA-spacer concentrations and below b) PL efficiencies of the same samples and c) PL$_{I.R.}$ shortly after PL$_0$ of the same samples using Equations (9) and (11) with the same parameters as in (a). The initial densities for $y = 0.8$ and $y = 1.0$ are corrected as described in the SOI.

**ADVANCED
SCIENCE NEWS**

www.advancedsciencenews.com

**ADVANCED
MATERIALS
INTERFACES**

www.advmatinterfaces.de

during the funneling of excitons into the local energy minima quantum wells from which the emission happens. The initial excited-state densities used for the fits of the $NMA_{0.8}$ and $NMA_{1.0}$ perovskites in Figure 5 are corrected using the fits shown and discussed in Figure S5 of the Supporting Information. The derived and calculated initial densities for the lowest fluence are assumed to be the same.

Comparing the parameters extracted in Table 1, although there is some spread in the trapping rate $k_{1,c}$, it tends to be on the order of the inverse of a few nanoseconds for the NMA samples. The trapping is fast and explains the increase in PL efficiency with increasing fluence even up to the highest fluences for all NMA samples (Figure 5b). The bimolecular rate constant increases by an order of magnitude from ≈ 5 to 50×10^{-10} cm^3 s^{-1} from $NMA_{0.4}$ to $NMA_{1.0}$. This is similar to the increase in γ_{EEA} for the increasing BA concentration, and indicates that the volume fraction of the total film that is made up of bandgap-minima QWs may be reduced by around an order of magnitude by this increase in the spacer concentration (assuming the microscopic bimolecular rates stay the same).

6. Discussion

The results in the previous sections suggest that the PL in quasi-2D perovskite films based on BA spacers tends to be dominated by excitons, with FCs beginning to play a role when BA spacer concentration decreases. On the other hand, FCs always dominate the PL of quasi-2D perovskites based on the NMA spacer. This would suggest that the local bandgap-minima QWs in the NMA film should be slightly larger. In Figure S7 of the Supporting Information we reproduce the emission spectra of the BA and NMA concentration series at low excitation fluences. Indeed, the emission of the NMA-based films is always lower in energy than the emission from the BA ones, consistent with lower-bandgap QWs being responsible for the emission in NMA irrespective of its concentration. In the BA series, the red-shifting of the emission with decreasing BA content is also consistent with an increasing contribution of larger local bandgap-minima QWs (and the associated FC emission).

We also note that the effective rate coefficients for bimolecular processes in quasi-2D perovskites increase as the 2D spacer concentrations increase. Although the microscopic annihilation rates inside the bandgap-minima quantum well could be influenced by confinement due to the size of the emitting QWs, some fraction of the change in the effective rates is likely related to a change in the volume fraction of the film that the bandgap-minima QWs constitute. As more thin QWs are created with higher 2D spacer concentrations, the bandgap-minima QWs may make up a lower fraction of the total film volume. Therefore, funneling into this smaller volume may lead to higher excited-state densities, and the estimation of N_0 for the occupied bandgap-minima QWs by considering the entire film volume will be increasingly erroneous. Although comparison of these effective rates is of merit, an even greater understanding of the materials could be gained if a better understanding of the volume fraction of QWs occupied after photoexcitation, and the microscopic rates therein could be gained. From current experimental work, it is not obvious how

such information can be gained, so further careful material and method development in this direction are of interest.

In terms of device understanding, these results establish the following salient points. Foremost, the nature of the excited states in quasi-2D perovskite films should be carefully considered. Our results suggest that it is incorrect to assume that excitons will always dominate the excited-state population in quasi-2D perovskites. Depending on the 2D spacers and their concentrations the excited-state population can vary widely from being exciton to free carrier dominated.

PeLEDs made from quasi-2D perovskite samples based on much lower concentrations of BA than used in this work are shown to exhibit high external quantum efficiencies of 10.1%.[25] Adding even small concentrations of BA leads to smoother surfaces and higher EQEs due to the increased radiative rate.[26] An increase in the BA molar ratio in MAPbBr$_3$ perovskites has been shown to improve the quantum yield from 0.2% at a molar ratio of $\gamma = 0$ up to 40.1% at $\gamma = 0.4$ and even at low current densities in PeLEDs based on BA the radiative recombination is faster than the nonradiative recombination.[27] Based on our observations the PL at these low BA concentrations is made up of both excitons and FCs. Increasing the excitonic PL contribution could lead to higher efficiencies by reducing the trapping.[28] However, an increase in BA concentration has been shown to increase shunt paths.[26] The smoothing of the energy transfer between the differently sized QWs has been shown to greatly increase the EQE up to 20.5% ($0.3 < x < 0.4$).[29] We suggest that increasing the excitonic contribution and therefore the BA concentration while avoiding shunt losses and losses in the funneling process can lead to highly efficient low current density PeLEDs.

For photovoltaic applications, where charge separation is required, the NMA-based materials would likely be favored. Indeed, recent work has investigated quasi-2D material using NMA spacers as the absorber material in solar cells, albeit with very large QWs, and using an organic cation and iodide. Introducing NMA increases the thermal stability of the perovskite[30] and the open-circuit voltage in solar cells leading to high power conversion efficiency.[31] The conjugated structure has been suggested to increase charge transfer between perovskite layers.[32] While NMA is suggested to decrease the trapping in perovskites,[30] we suggest not to increase the concentration beyond $\gamma = 0.6$ based on our observations. Increasing the NMA concentration while avoiding fast trapping could lead to highly efficient and stable solar cells.

7. Conclusion

We demonstrate that the time-resolved PL characteristics of quasi-2D materials vary significantly between BA and NMA 2D spacers and also with the concentration of a given spacer. The TRPL dynamics cannot in general be explained by a model considering only excitons or only free charge carriers. The simplest model we can propose that consistently explains the data involves two independent pools, an FC pool, and an exciton pool. This model can then explain the fluence dependence of the TRPL dynamics, initial PL rate, and the PLQY. For high concentrations of the NMA spacer, this model must be augmented to allow some higher-order population loss within the instrument response.

For the BA spacer, we obtain monomolecular exciton recombination rates of 2.6×10^7 to 4.7×10^7 s^{-1} remaining essentially unaffected by the change of molar BA ratio from $\gamma = 0.4$ to $\gamma = 1.0$. At the same time, the effective EEA rate changes from 0.75×10^{-10} to 60×10^{-10} cm^3 s^{-1} increasing continuously and significantly as the BA concentration increases. The effective rate is calculated based on the assumption of a uniform excited state density across the whole film. We ascribe a large part of the change in the effective rate to a decreasing validity of this assumption with increasing BA content (rather than a major change in the real diffusion rate or size of the excitons). Unfortunately, as the actual volume of the film to which the excited states are constrained is not known, the true rates of EEA cannot be extracted. This open question is worth further experimental consideration, with some novel ideas necessary to provide the observations that would allow this question to be answered. At lower BA contents, an FC population significantly contributes to the PL. The FC population is much shorter-lived than the exciton population (consistent with the observations for NMA). The effective k_2 extracted are 3.7×10^{-10} to 19×10^{-10} cm^3 s^{-1}, which are higher than the 10^{-10} cm^3 s^{-1} typically observed in 3D perovskites[33] and again increase with increasing BA concentration. These increased effective k_2 rates are consistent with our explanation for the effective EEA rates mentioned above.

For the NMA spacer, we observe effective k_2 rates between 4.7×10^{-10} and 50×10^{-10} cm^3 s^{-1} increasing with the NMA concentration. We contribute this to the same mechanism as with the BA spacer. The fast trapping (10^9 s^{-1}) causes efficiencies to increase even at high excitation fluences as radiative recombination becomes more dominant. We find that the absence of a long-lived PL contribution at high NMA concentrations in combination with a power-law slope of the initial PL smaller than two is likely due to excited-state loss mechanisms during the funneling process as opposed to higher excitonic PL contributions. The TRPL can be reasonably fit with just FC recombination, meaning that excitonic contribution in NMA-perovskites plays a minor role.

In summary, we show that the TRPL of quasi-2D perovskites is not trivial and can have exciton and free charge carrier recombination characteristics depending on the spacer molecule and concentration. We demonstrate how simultaneous emission from two separate excitons and free charge carrier pools can explain our observation. Further understanding of the emitting QWs and the excited-state funneling process are promising topics for potential device improvement in the future.

8. Experimental Section

Perovskite Fabrication: The spacers used in this work are BA and NMA. The spacer concentrations are given in fraction of elemental composition so $\gamma = 0.4$. BA represents CsPbBr$_3$(BABr)$_{0.4}$. The films were prepared in the same manner as the ones from Li et al.[24] A mixture of 5.3 mg 12-Crown-4 and 239.1 mg CsPbBr$_3$ were dissolved in 1 mL of DMSO and heated for ≈20 min at 60 °C. Then either BABr/DMSO (2.8 м) or NMABr/DMSO (2.8 м) solution was added in the quantity needed to reach the desired elemental composition. The solutions were spin-coated on glass substrates utilizing a consecutive two-step process at 1000 rpm (ramp rate: 1000 rpm s^{-1}) for 20 s followed by 4000 rpm (ramp rate: 1000 rpm s^{-1}) for 40 s. Finally, the films were annealed for 10 min at 70 °C.

Characterization: For the measurement of the PL dynamics a femtosecond laser and third harmonic generation was used to excite the samples (Light Conversion, Pharos/Hiro), and a streak camera (Hamamatsu Universal C10910) combined with a spectrometer (Acton SpectraProSP2300) was used to measure the TRPL. The excitation wavelength was 342 nm with a repetition rate of 1 kHz and a pulse width of 260 fs. The spot size was 7.8×10^{-3} cm^2 as measured with a beam profiler (Thorlabs). The PL was collimated using a 5 cm diameter lens with a 10 cm focal length before being focused on the spectrometer. To collect TRPL dynamics the number of photons per pixel per acquisition time was recorded. The streak camera gain settings and sample position were kept the same while the excitation fluence was changed to allow comparison over the fluence series. However, to avoid overexposure ND filters were used between the sample and the streak camera to attenuate the emission appropriately. The measured values were then corrected for known attenuation of the ND filter used.

Fitting: For Figures 3a,b, 4a, and 5a the data are globally fitted in Origin (OriginLab). A nonlinear weighted least squares regression with the weights: $w_i = \frac{1}{y_i}$ was used. The rate parameters were shared across each fluence series fit. The iteration method is used for the Levenberg–Marquardt algorithm, which provides an estimate of the standard errors in the fitted parameters by an analysis of the variance-covariance matrices. These standard errors in the fit parameters are quoted in the text.

Supporting Information

Supporting Information is available from the Wiley Online Library or from the author.

Conflict of Interest

The authors declare no conflict of interest.

Data Availability Statement

The authors gratefully acknowledge funding from the DFG (PEROLAS, No. 409035484) and the Karlsruhe School of Optics & Photonics (KSOP).

**ADVANCED
SCIENCE NEWS**

www.advancedsciencenews.com

**ADVANCED
MATERIALS
INTERFACES**

www.advmatinterfaces.de

[1] J. Calabrese, N. L. Jones, R. L. Harlow, N. Herron, D. L. Thorn, Y. Wang, *J. Am. Chem. Soc.* **1991**, *113*, 2328.

[2] P. Tyagi, S. M. Arveson, W. A. Tisdale, *J. Phys. Chem. Lett.* **2015**, *6*, 1911.

[3] N. Wang, L. Cheng, R. Ge, S. Zhang, Y. Miao, W. Zou, C. Yi, Y. Sun, Y. Cao, R. Yang, Y. Wei, Q. Guo, Y. Ke, M. Yu, Y. Jin, Y. Liu, Q. Ding, D. Di, L. Yang, G. Xing, H. Tian, C. Jin, F. Gao, R. H. Friend, J. Wang, W. Huang, *Nat. Photonics* **2016**, *10*, 699.

[4] L. Cheng, Y. Cao, R. Ge, Y.-Q. Wei, N.-N. Wang, J.-P. Wang, W. Huang, *Chin. Chem. Lett.* **2017**, *28*, 29.

[5] L. Cheng, T. Jiang, Y. Cao, C. Yi, N. Wang, W. Huang, J. Wang, *Adv. Mater.* **2020**, *32*, 1904163.

[6] J. Byun, H. Cho, C. Wolf, M. Jang, A. Sadhanala, R. H. Friend, H. Yang, T.-W. Lee, *Adv. Mater.* **2016**, *28*, 7515.

[7] Z. Ren, J. Yu, Z. Qin, J. Wang, J. Sun, C. C. S. Chan, S. Ding, K. Wang, R. Chen, K. S. Wong, X. Lu, W.-J. Yin, W. C. H. Choy, *Adv. Mater.* **2021**, *33*, 2005570.

[8] Y. Jiang, J. Wei, M. Yuan, *J. Phys. Chem. Lett.* **2021**, *12*, 2593.

[9] M. Yuan, L. N. Quan, R. Comin, G. Walters, R. Sabatini, O. Voznyy, S. Hoogland, Y. Zhao, E. M. Beauregard, P. Kanjanaboos, Z. Lu, D. H. Kim, E. H. Sargent, *Nat. Nanotechnol.* **2016**, *11*, 872.

[10] W. Bi, Q. Cui, P. Jia, X. Huang, Y. Zhong, D. Wu, Y. Tang, S. Shen, Y. Hu, Z. Lou, F. Teng, X. Liu, Y. Hou, *ACS Appl. Mater. Interfaces* **2020**, *12*, 1721.

[11] Y. Han, S. Park, C. Kim, M. Lee, I. Hwang, *Nanoscale* **2019**, *11*, 3546.

[12] X. Yang, X. Zhang, J. Deng, Z. Chu, Q. Jiang, J. Meng, P. Wang, L. Zhang, Z. Yin, J. You, *Nat. Commun.* **2018**, *9*, 570.

[13] B. Zhao, S. Bai, V. Kim, R. Lamboll, R. Shivanna, F. Auras, J. M. Richter, L. Yang, L. Dai, M. Alsari, X.-J. She, L. Liang, J. Zhang, S. Lilliu, P. Gao, H. J. Snaith, J. Wang, N. C. Greenham, R. H. Friend, D. Di, *Nat. Photonics* **2018**, *12*, 783.

[14] M. Ban, Y. Zou, J. P. H. Rivett, Y. Yang, T. H. Thomas, Y. Tan, T. Song, X. Gao, D. Credgington, F. Deschler, H. Sirringhaus, B. Sun, *Nat. Commun.* **2018**, *9*, 3892.

[15] Y. Miao, L. Cheng, W. Zou, L. Gu, J. Zhang, Q. Guo, Q. Peng, M. Xu, Y. He, S. Zhang, Y. Cao, R. Li, N. Wang, W. Huang, J. Wang, *Light: Sci. Appl.* **2020**, *9*, 89.

[16] X. Hong, T. Ishihara, A. V. Nurmikko, *Phys. Rev. B* **1992**, *45*, 6961.

[17] T. Ishihara, *J. Lumin.* **1994**, *60–61*, 269.

[18] J. C. Blancon, A. V. Stier, H. Tsai, W. Nie, C. C. Stoumpos, B. Traoré, L. Pedesseau, M. Kepenekian, F. Katsutani, G. T. Noe, J. Kono, S. Tretiak, S. A. Crooker, C. Katan, M. G. Kanatzidis, J. J. Crochet, J. Even, A. D. Mohite, *Nat. Commun.* **2018**, *9*, 2254.

[19] C. C. Stoumpos, D. H. Cao, D. J. Clark, J. Young, J. M. Rondinelli, J. I. Jang, J. T. Hupp, M. G. Kanatzidis, *Chem. Mater.* **2016**, *28*, 2852.

[20] J. Cho, J. T. DuBose, P. V. Kamat, *J. Phys. Chem. Lett.* **2020**, *11*, 2570.

[21] C. L. Davies, M. R. Filip, J. B. Patel, T. W. Crothers, C. Verdi, A. D. Wright, R. L. Milot, F. Giustino, M. B. Johnston, L. M. Herz, *Nat. Commun.* **2018**, *9*, 293.

[22] L. Lei, D. Seyitliyev, S. Stuard, J. Mendes, Q. Dong, X. Fu, Y.-A. Chen, S. He, X. Yi, L. Zhu, C.-H. Chang, H. Ade, K. Gundogdu, F. So, *Adv. Mater.* **2020**, *32*, 1906571.

[23] G. Delport, G. Chehade, F. Lédée, H. Diab, C. Milesi-Brault, G. Trippé-Allard, J. Even, J.-S. Lauret, E. Deleporte, D. Garrot, *J. Phys. Chem. Lett.* **2019**, *10*, 5153.

[24] Y. Li, I. Allegro, M. Kaiser, A. J. Malla, B. S. Richards, U. Lemmer, U. W. Paetzold, I. A. Howard, *Mater. Today* **2021**.

[25] P. Vashishtha, M. Ng, S. B. Shivarudraiah, J. E. Halpert, *Chem. Mater.* **2019**, *31*, 83.

[26] L. Xu, Y. Qiang, H. Hu, P. Lin, P. Wang, S. Che, H. Sun, Z. Nie, C. Cui, F. Wu, D. Yang, X. Yu, *Nanotechnology* **2019**, *30*, 105703.

[27] Z. Xiao, R. A. Kerner, L. Zhao, N. L. Tran, K. M. Lee, T.-W. Koh, G. D. Scholes, B. P. Rand, *Nat. Photonics* **2017**, *11*, 108.

[28] F. Li, L. Yang, Z. Cai, K. Wei, F. Lin, J. You, T. Jiang, Y. Wang, X. Chen, *Nanoscale* **2018**, *10*, 20611.

[29] L. Kong, X. Zhang, Y. Li, H. Wang, Y. Jiang, S. Wang, M. You, C. Zhang, T. Zhang, S. V. Kershaw, W. Zheng, Y. Yang, Q. Lin, M. Yuan, A. L. Rogach, X. Yang, *Nat. Commun.* **2021**, *12*, 1246.

[30] B. Chaudhary, T. M. Koh, B. Febriansyah, A. Bruno, N. Mathews, S. G. Mhaisalkar, C. Soci, *Sci. Rep.* **2020**, *10*, 429.

[31] C.-T. Lin, J. Lee, J. Kim, T. J. Macdonald, J. Ngiam, B. Xu, M. Daboczi, W. Xu, S. Pont, B. Park, H. Kang, J.-S. Kim, D. J. Payne, K. Lee, J. R. Durrant, M. A. McLachlan, *Adv. Funct. Mater.* **2020**, *30*, 1906763.

[32] J. Chang, S. Zhang, N. Wang, Y. Sun, Y. Wei, R. Li, C. Yi, J. Wang, W. Huang, *J. Phys. Chem. Lett.* **2018**, *9*, 881.

[33] I. Allegro, Y. Li, B. S. Richards, U. W. Paetzold, U. Lemmer, I. A. Howard, *J. Phys. Chem. Lett.* **2021**, *12*, 2293.